

Robotics Group  
The Maersk Mc-Kinney Moller Institute  
University of Southern Denmark

---

Technical Report no. 2007 – 5

---

# **Using Tactile Sensors for Multisensorial Scene Exploration**

Morten Kjærgaard, Alex Bierbaum, Dirk Kraft, Sinan Kalkan, Norbert Krüger, Tamim  
Asfour, Rüdiger Dillmann

January 22, 2007

Title Using Tactile Sensors for Multisensorial Scene Exploration

Copyright © 2007 Morten Kjærgaard, Alex Bierbaum, Dirk Kraft, Sinan Kalkan, Norbert Krüger, Tamim Asfour, Rüdiger Dillmann. All rights reserved.

Author(s) Morten Kjærgaard, Alex Bierbaum, Dirk Kraft, Sinan Kalkan, Norbert Krüger, Tamim Asfour, Rüdiger Dillmann

Publication History

# 1 Introduction

This paper explores the usage of two relatively cheap industrial haptic sensors to extend visual scene exploration to a multisensorial scene exploration. It takes a look at the extraction of different object properties and how these can be used to augment the existing visual representation of the environment.

Section 2 gives an overview of the requirements for a sensor for haptic exploration and the electrical characteristics of the considered sensors and the measurement electronics. In section 3 the physical properties of the sensor are shown and its step response and a resulting linearization are derived. Section 4 presents different experiments and approaches towards extracting surface normals, weight information and elasticity from the sensor data. The fusion of visual predicted surface information with haptical surface exploration is shown in section 5.

## 2 Hardware

### 2.1 Choice of the Tactile Sensor Type

The purpose of the tactile sensor system is the support of haptic exploration and controlled grasping skills for the robot. The following requirements arise from this application:

**High sensitivity and wide measurement range:** Detection of slight contacts of a few gram weight equivalent should be possible, but the sensor must also not be overdriven when moving or lifting weights in the range of 1–2 Kg.

**Response dynamics:** The sensor signal should have a rise time below 20 ms to allow the implementation of controlled grasping.

**Reliability:** A strong demand for the choice of the sensor is a proven sensor technology which affords little maintenance and has a sufficient life time.

**Size and ease of integration:** The sensor device should be small enough to fit into the phalanxes of the Karlsruhe Robot Hand [6], which is of the size of the human hand.

**Electrical interface and measurement electronics:** The sensor should provide an electrical interface with low cable count and that is not sensitive towards moderate electrical interference. The measurement electronics must be small in size and should offer a standard PC communication interface like RS232 or USB.

Beside these basic demands a further strong requirement for the tactile sensors is the capability to determine the contact normal force vector (CNFV) which allows for dextrous manipulation and reactive grasping with several common control algorithms.

For the tactile sensor system several sensor types have been investigated for their suitability. Sensors for force measurement may be divided in scalar and matrix type sensors. Using matrix force sensors the CNFV may be approximated from the measurement data when assuming a contact area larger than the sensors' grid resolution. Manufacturers of commercial matrix type force sensors are [3][2][4]. These sensors are usually manufactured as flexible sheets with uniformly distributed adjacent sensor cells. The cells usually have the shape of squares with the length of an edge ranging down to a few millimeters, defining the resolution. There is no off-the-shelf solution available for matrix force sensors in the application area of robot hands. The sensors always need to be customized in terms of geometry and resolution, which results in considerable costs for this type of sensor. All manufacturers examined require the customer to use a special sensor signal

processing hardware unit for processing sensor data. The sensor technology used for force sensors relies either on a variant of the FSR (Force Sensing Resistor) principle [3][4][1] or on the capacitive effect [2].

FSRs are also very common in tactile input devices like keyboards and keypads for PCs or hand-held devices. Sensor design and properties are in a technological mature state which allows immediate deployment of this sensor for tactile force and contact sensing to the required degree.

Although the term FSR itself is copyrighted by [1] the other manufacturers exploit material properties in a similar way, so that they are summarized under this term. The FSR sensor itself consists of two polymer sheets, one with a printed conducting electrode pattern and one with a semiconducting layer [7]. The resistance of the sensor decreases with increasing pressure applied to it as the two sheets are pressed together. The force sensing resistor is despite its name neither a pure force nor a pure pressure sensor. Its change in resistance is related to the portion of sensor surface addressed, the elasticity of the actuator and the electrode design on the sheet. The sensor element can be used as a pressure sensor if the force is applied to a major portion of the sensor area. This can be achieved by an appropriate actuator that distributes the force equally to the full sensor area. As a tactile sensor for a robot hand it is sufficient to overlay a spherical layer of an elastomer as actuator element on top of the sensor surface. The response time of an FSR is in the range of 1–2 ms, which is sufficient for tactile exploration and CNFV control.

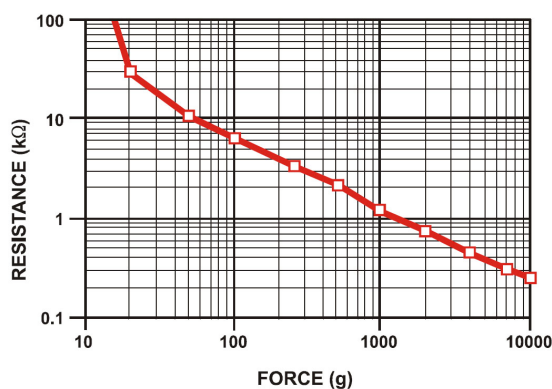


Figure 1: FSR Characteristics: Resistance vs. Force [1].

FSRs in general require a break force to switch from zero conductivity to a finite resistance value defining the beginning of the dynamic range. From here the characteristic usually follows an inverse power law as shown in the double logarithmic plot in figure 1.

This nonlinear resistance-force relation needs to be linearized by calibration if required for quantitative measurements.

## 2.2 Cursor Navigation Sensors for Tactile Sensing

Beside 1-D FSR elements for orthogonal contact force measurement the FSR technology is also used in cursor navigation devices as they are assembled in hand-held devices or laptop computers. These sensor devices have four FSR elements arranged in quadrants onto which the force is distributed by an actuator stick as shown in figure 2. The stick is covered with a rubber cap to provide friction during actuation.

When the actuator stick is bent the applied force is distributed and the resistance value of the four sensor elements change uniquely to the 2-D angle and the magnitude of the force.

After linearization of the resistance value for each quadrant the CNFV may be calculated as the resulting force from the four measurement values.



Figure 2: *MicroJoystick* input device [1].

A disadvantage of the sensor assembly is the actuator stick itself as it can not be integrated satisfactorily into a robot hand. It sticks out of the hand plane which makes it vulnerable against force overload. Also, the measurement range of the sensor is not sufficient towards smaller forces. Experiments have shown that the break force of the sensor device is the equivalent of approximately 70 gram weight. This is not sufficient to detect contact immediately or to control the CNFV with detailed resolution. Further more the electrical connection is only possible with a special flex board style connector that has to be glued with conductive adhesive to the contacts of the sensor, which increases the number of steps necessary for assembly.

Despite these issues the sensor may well be deployed to explore haptical features of objects in contact with the robot hand. This sensor was integrated into a two jaw gripper to investigate its properties and suitability for tactile exploration and reactive grasping, details will be shown later in this report.

Meanwhile also the mere four quadrant sensor element without actuator is available for purchase.

This FSR device is directly solderable to a PCB, alternatively copper wires may be soldered to the sensor. For proper operation the sensor needs to be used in conjunction with an actuator element. With this sensor it is sufficient to cover it with a spherical elastomer layer that distributes the applied force across the sensing area. The sensitivity can be adjusted by shape, thickness and elasticity of the elastomer layer. Experiments have shown that this sensor device can measure down to the force equivalent of 5 gram weight by overlaying a spherical silicone cap as shown in figure 3.

The upper limit of the measurement range is approximately the equivalent of 1.5 Kg.

The package of the *MicroNav 360* [1] sensors also make them a suitable base element for tactile matrix sensors as they can be arranged as grids on a carrier PCB.

### 2.3 Sensor Electronics and System Integration

By using a simple voltage divider circuit a measurable voltage signal can be generated from the changing resistance value of the FSR. The resistance value of the FSR ranges from 5 k $\Omega$  at high forces to approximately 100 k $\Omega$  at forces just above the break force point. The voltage signals of the sensors are directly connected to ADC inputs of a microcontroller. The microcontroller communicates to a host PC via a standard interface,

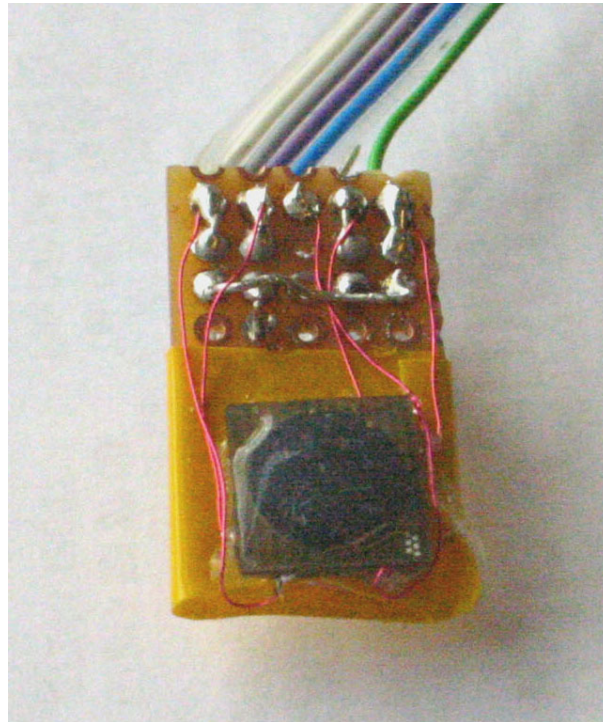


Figure 3: *MicroNav 360* with silicon cap and carrier board.

e.g. RS232, CAN or Bluetooth. This data acquisition circuit is generic and may be used for all types of FSR sensors. The microcontroller is used as a measurement unit and does not calculate a calibration function on the acquired measurement data. This is performed by software running on the connected PC for ease of software maintainability.

Figure 4 shows a jaw gripper equipped with cursor navigation sensors. Here four devices were soldered to a PCB to investigate the feasibility of a matrix sensor field.

The data acquisition circuit is attached to the backside of one jaw, also the typical flex board cables as needed for the *MicroJoystick* device [1] are visible. This setup is used as a demonstrator for investigating the characteristics of the *MicroJoystick* cursor navigation sensor in tactile exploration. As mentioned before the bulky geometry of the sensors actuator cap and the connection wires make this setup sensitive towards mechanical damage. Also, the grippers contact area is reduced to the actuator caps front surface which is not suitable for clamping objects.

In a second approach cursor navigation sensors with silicone actuator caps were integrated into a humanoid robot hand [6].

Figure 5 shows the FSR sensor element integrated into the thumb tip of the humanoid robot hand. The active sensor area is covered with a thin layer of silicone that was adapted to the shape of the underlying silicone finger tip. This silicone cap naturally flows to a spherical shape which results in a proper actuator for this sensor. An advantage of this design is that the finger surface area is not affected by the integration of the sensor and the stable mechanical design of the finger tips can be maintained.

First experiments approve this integrated tactile sensor a high sensitivity in the desired range from approximately 10 gram up to more than a Kilogram weight. Upcoming investigations will determine to what resolution this sensor design permits reliable tactile exploration and grasp control.

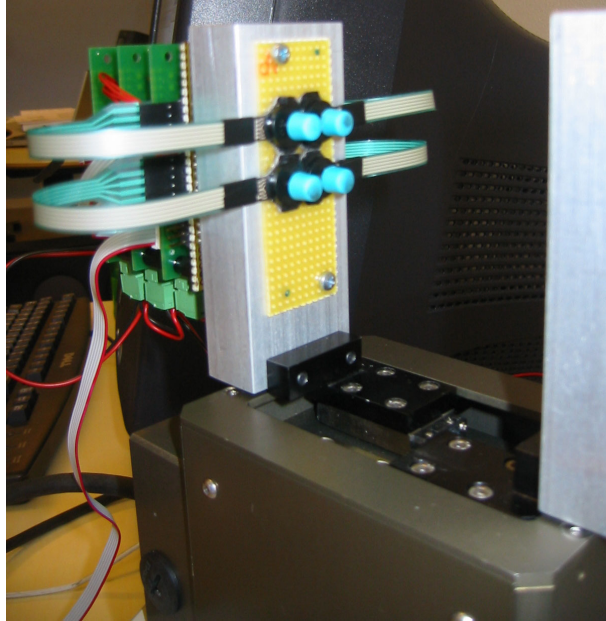


Figure 4: Four *MicroJoystick* devices mounted to a jaw gripper.



Figure 5: Integration of *MicroNav 360* sensor device .

### 3 Basic sensor properties

This chapter will go into more details of the properties and characteristics of the *MicroJoystick* sensor.

#### 3.1 Physical properties

The sensor is mounted on a piece of PCB which acts as a base plate for further mounting, and also gives a pinout of the electric terminals from the four internal FSR sub-sensors. The dimensions of this base plate is shown in figure 6(a) and figure 6(b), and the pinout of the electric terminals can be seen in figure 2 as 5 traces.

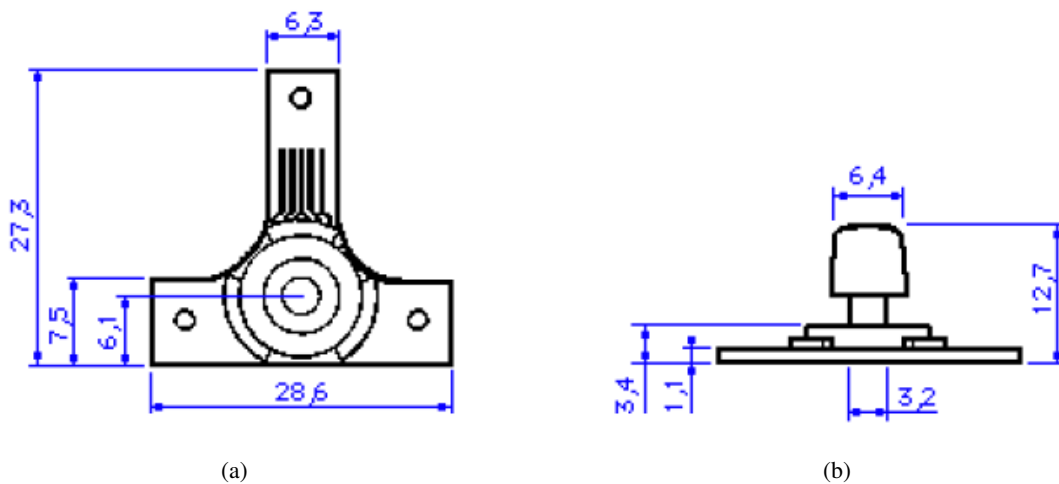


Figure 6: MicroJoystick Sensor Dimensions [mm]. (a) Top View. (b) Side view

#### 3.2 Step-response

Our first approach in analyzing the sensor was to get a step response by applying a normal force on the sensor simply by slowly bringing the sensor in contact with a flat surface and keeping it steady.

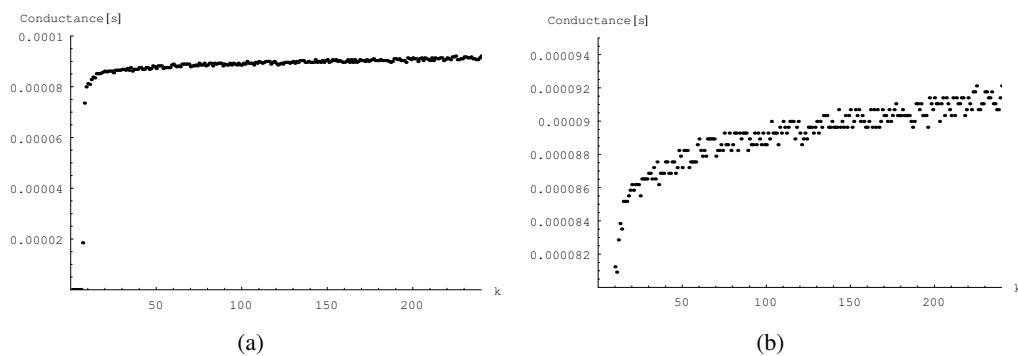


Figure 7: Step response.  $k$ =sampling. Sampling time is 10Hz. (a) Full Range. (b) Magnification of the small force range.

The signal from each of the four sub-sensors was sampled with a frequency of 10Hz, and the measurements from one of the sub-sensors is plotted in figure 7(a). The moment the sensor makes contact with the surface

the signal grows rapidly. Afterwards the signal actually keeps growing slowly even if the sensor is kept in a constant position. Figure 7(b) gives a more detailed impression of the same measurements. The plot show the signal over a period of about 20 seconds,. Further tests have shown that the signal actually keeps growing for up to about 60 seconds.

### 3.3 Linearization

The purpose of linearization is to discover a function that can convert the measured sensor signal to a force value, within a suitable error interval. The input to this function will be the measured signal from the sensor. The physical property of the sensor that can be measured is the resistance of each FSR, which is converted into a voltage  $s$  in the interval 0–5 V using a voltage divider.

One possibility would be to directly translate this voltage into a force value using an approximated function  $f_v$  of the form in equation 1.

$$force = f_v(s) \quad (1)$$

This has the drawback that the resistance  $R$  of each sub-sensor is translated into a voltage in a non-linear way using the voltage-divider relationship. This means that we lose the linear relationship between the measured resistance and the force.

To take advantage of this expected linear property we could calculate the resistance from the voltage, and try to find a function that translates this into a force. Even better is to use the conductance, since it has a nice and close to linear relationship to the force. This gives a relation as shown in equation 2.

$$force = f_c\left(\frac{1}{R}\right) \quad (2)$$

Since the sensor is expected to have a linear relationship in the low force region, the function is expected to have the form shown in equation 3. For higher forces a higher order function might be needed to get a suitable approximation.

$$f_c(x) = \alpha + \beta \cdot x \quad (3)$$

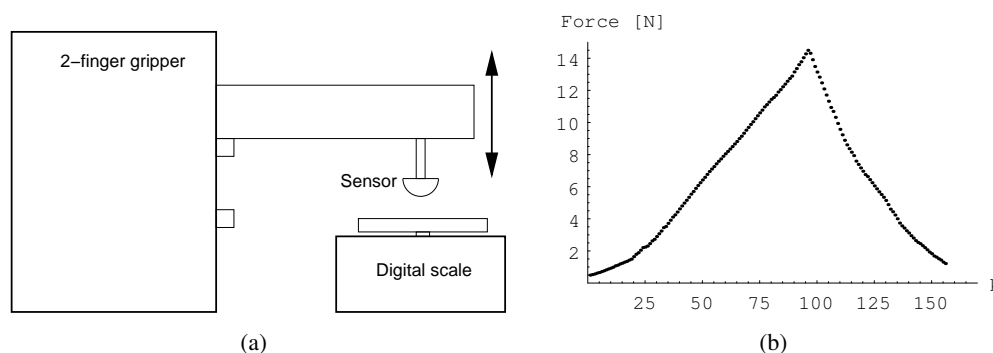


Figure 8: Linearization Experiment. **(a)** Setup for the linearization experiment. **(b)** Magnitude of the applied force during each sampling  $k$ .

To collect a number of measurements from the sensor with a known force applied, a digital scale was used to measure the force. The experiment was carried out by mounting a sensor on one of the fingers of a parallel gripper, so that the sensor was pointing downwards and could be moved up and down. The digital scale was

placed under the sensor, and by changing the position of the finger the sensor would apply a force on the scale which could be measured. This setup is shown in figure 8(a).

The sensor was moved closer to the scale in small steps. In each position the total force was measured with the digital scale, and the four reading from the four sub-sensors were recorded. This gave an increasing force on the sensor in each step. After a force of about 14 N was reached, the inverse experiment was made by slowly moving the sensor away and thereby decreasing the force in slow steps. This resulted in 156 measurements. The applied force measured with the scale is shown in figure 8(b).

The force was applied as a normal force, so we would expect equal readings from all four sub-sensors. The mathematical distribution of the force is shown in figure 9. Since the sensor consists of four sub-sensors, the force should be equally distributed over these so that each will measure a force of  $F_i = \frac{1}{4}F$ , where  $F_i \in \{F_N, F_S, F_E, F_W\}$ .

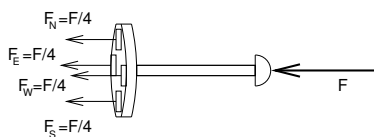


Figure 9: Distribution of force on the sub-sensors when a normal force is applied

### 3.3.1 Experiment Data

Figure 10 shows the results from the North sub-sensors. The force on the x-axis is  $\frac{1}{4}$  of the total force measured with the scale, since this should be the theoretical magnitude of force that is applied to one sub-sensor. The red marks are the results from the first part of the experiment when the force was increasing, and the blue marks are from the last part where the force was decreasing. During the last part of the experiment the sensor seems to have higher readings than when the force is increasing. It was shown that the sensor readings would keep increasing when a force was applied to the sensor over a period of time, and it seems to be the same characteristic that is the reason for the different readings in figure 10. During the experiment the sensor was subject to a high force, and this large force would make the sensor readings higher during the last part of the experiment.

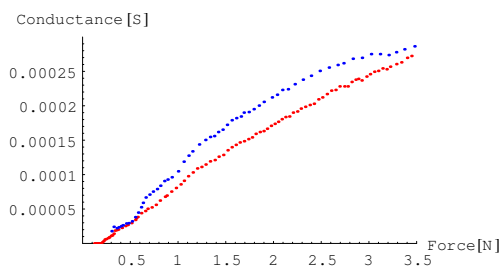


Figure 10: Measured conductance from the north sub-sensor during linearization experiment. **Blue:** Decreasing force. **Red:** Increasing force

Figure 10 shows that the relationship doesn't follow a straight line over the measured range, but more a second order relationship.

In the low-force range it would be possible to approximate the relationship with a first order function, which might not give the same accuracy as a second order but would be preferred for the following reasons:

- Individual sensor calibration is easier and requires less data points.
- FSR sensors have low accuracy, so the loss of precision by using a 1st order relationship does not make a significant difference.

Since the characteristic of FSR sensors differs very much from part to part, an easy way to calibrate individual sensors would probably give a better accuracy than an uncalibrated sensor with a higher order approximation. And since forces as high as the experiment tested (up to 14 N) will not be needed in the current application, it would be better to linearize the sensors in the low force range using a first order relationship.

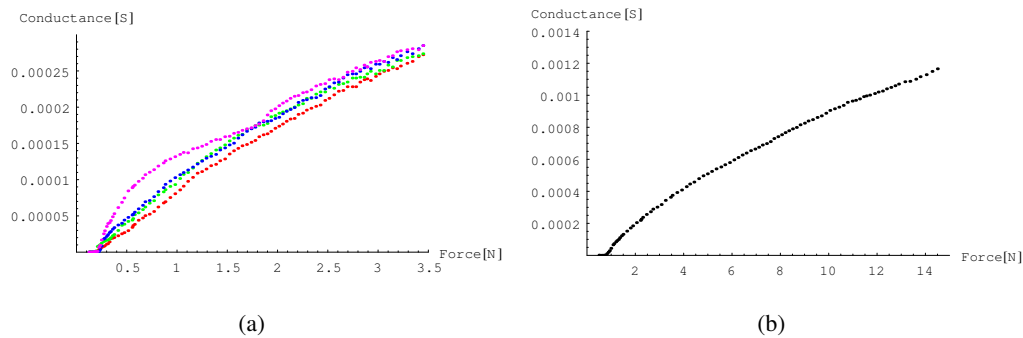


Figure 11: Measured conductance from all sensors during linearization experiment with only increasing force. **(a)** Conductance from each sub-sensors. Red=North, Blue=South, Green=East & Purple=West. **(b)** Sum of the conductance from all sub-sensors.

The data points from the part of the experiment with increasing force from all four sub-sensors are shown in figure 11(a). The graph representing the W sub-sensor, is growing clearly faster than the other 3 sub-sensors, which is an unexpected behavior. The other 3 sub-sensors have a slight difference in measured force, with the red graph (North), lying a little lower than the last two: blue (South) and green (East). Since the force was applied as a normal force, equal readings from all 4 sub-sensors would have been expected. The reason for the differences could be:

- Differences in the characteristics of each individual FSR sub-sensor
- The force was not exactly normal, but had a tangential component due to surface friction

The difference in the characteristics for each sub-sensor could be overcome by calibrating each sub-sensor individually, by assuming equal distribution of force on each sub-sensor, and then approximating the force-conductance relationship individually for each sensor.

But several other experiments of the same kind showed that it was not the same sub-sensor that gave the highest reading each time. This shows that the differences was due to a tangential force acting on the sensor-tip, and tilting the actuator slightly. Since an tangential force will tilt the actuator, it will apply a torque on the sensor. This torque will give a force acting on the N and S sub-sensor with the same magnitude, but in different directions. The same holds for the W and E sensor. This means the effect of the tangential force could be minimized by using the sum of the 4 sub-sensor readings. This sum is plotted in figure 11(b) against the total force.

Because of the intended application datapoints above 8 N will be disregarded in the following. The remaining datapoints are approximated to a straight line using least-squares approximation. This gives a

force-conductance relationship as shown in equation 4. The inverse which should be used to calculate the force from a measured conductance is shown in equation 5.

$$C(f) = -3.9336 \cdot 10^{-6} + 100.5 \cdot 10^{-6} \cdot f \quad (4)$$

$$F(c) = 0.0391384 + 9949.88 \cdot c \quad (5)$$

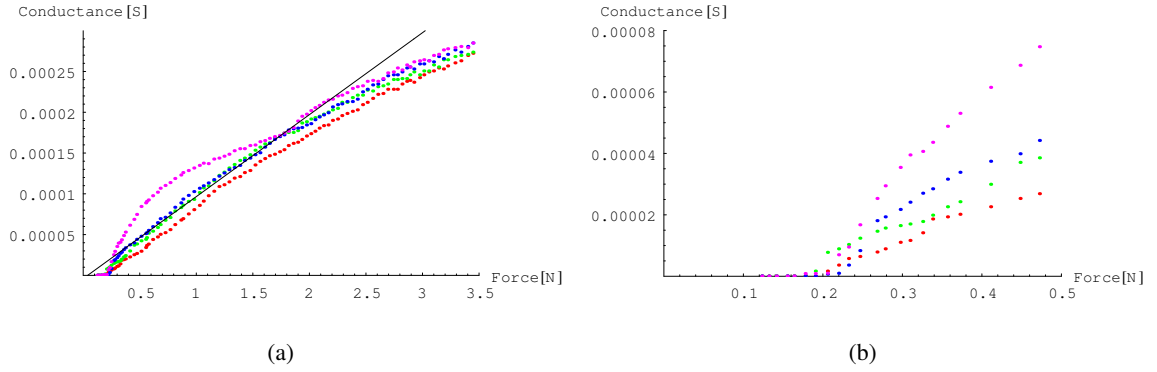


Figure 12: Measured conductance from all sensors during linearization experiment with only increasing force. Red=North, Blue=South, Green=East & Purple=West. **(a)** Result of linearization compared to the measured results. **(b)** Magnification of the low force range shows the magnitude of the break force.

In figure 11(a) you also see the result of the break force required to get readings from the sensor. With very low forces applied there is no reading from the sensor. This situation is more clearly shown in figure 12(b) which is a magnification of the small force range of figure 11(a). This shows that the break force for each sub-sensor is approximately  $0.2N$ , which means that a minimum force of  $0.8N \approx 80g$  is required if it is applied as a normal force, and the force is equally distributed over the 4 sub-sensors.

### 3.4 Sensor Model

To better understand and interpret the signals from each sensor, we have created a theoretical and simplified model of the sensor. It can be used to calculate the expected signal from the sensor when a known force is applied and vice versa.

To simplify the model we have made the following assumptions:

1. Each sub-sensor measures a force in only one point
2. Each sub-sensor measures only the perpendicular component of the force in this point
3. The contact point is always assumed to be the point at the end of the tip
4. A tangential force will contribute to a torque around a fixed rotation point

To calculate how much a force vector applied at the end of the tip contributes to the internal force sensors, we split the force-vector into the normal and tangential component. The normal component is shown in figure 13(a). Since the contact point is assumed to be in the middle of the sensor-tip, the normal component will be equally distributed over the four sub-sensors.

The tangential component is a little more complicated. Since the sub-sensors only measure a normal force, they do not directly detect the tangential component. But according to assumption three, this force will contribute to a torque around a fixed point, which is assumed to be in the middle of the sensor. The distance from the tip to this center of rotation is defined as  $l1$ , and depends on the geometry of the sensor. Since the sub-sensors only measure the force in one single point, this torque will give a force in each sub-sensor depending on the distance from the center of rotation to the location of the sub-sensor. This distance is defined as  $l2$ . This is shown in figure 13(b).

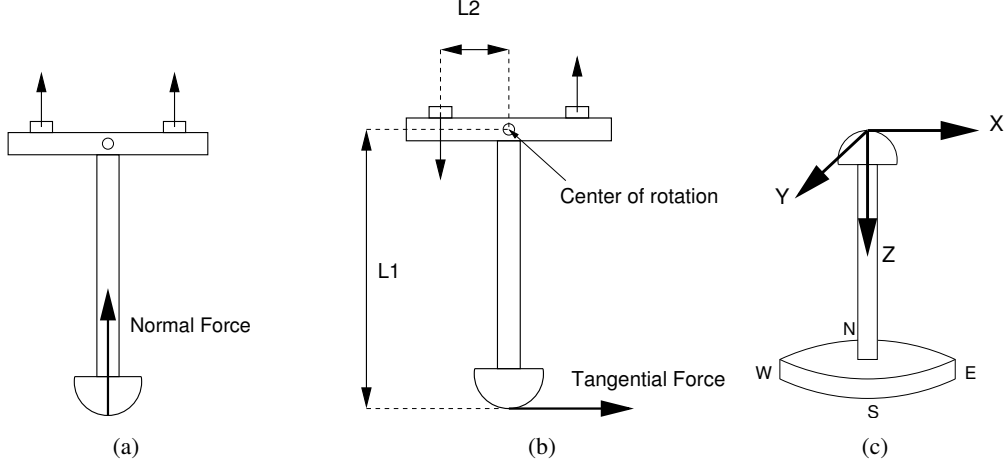


Figure 13: Distribution between the subsensors of a force applied to the sensor tip. **(a)** Force normal to the sensor **(b)** Force tangential to the sensor **(c)** Definition of the sensor frame

### 3.4.1 From force to sensor measurements

We assume the applied force vector is specified in the frame of the sensor which is defined with the origin at the tip of the sensor, the z-axis pointing towards the base and the x-axis in the direction of the East sub-sensor as shown in figure 13(c).

If the force vector is defined as  $(x, y, z)^T$ , the normal component is simply the z-component. The contribution to each of the 4 sub-sensors from the normal component is shown in equation 6.

$$n_{normal} = s_{normal} = e_{normal} = w_{normal} = \frac{1}{4}z \quad (6)$$

The Y-component results in a torque that is measured by the N and S sub-sensor, and the X-component gives a torque measured by the E and W sub-sensors. For example is the torque due to the X-component of the force is  $T = l1 \cdot x$ , and the magnitude of the force measured by the E sub-sensor due to this torque  $E_{tangent} = \frac{1}{l2} \cdot T = \frac{l1}{l2} \cdot x$ . I define the relationship  $\frac{l1}{l2}$  as  $\alpha$  which gives the results shown in vector form in equation 7.

$$\begin{pmatrix} n \\ s \\ e \\ w \end{pmatrix}_{tangent} = \alpha \cdot \begin{pmatrix} -y \\ y \\ x \\ -x \end{pmatrix} \quad (7)$$

The total force measured by each sub-sensor is shown in equation 8.

$$\begin{pmatrix} n \\ s \\ e \\ w \end{pmatrix} = \alpha \cdot \begin{pmatrix} -y \\ y \\ x \\ -x \end{pmatrix} + \frac{1}{4}z \quad (8)$$

### 3.4.2 From sensor measurements to force

The method to calculate the expected sensor output due to a known force is informal. Since the force vector consists of 3 unknowns and the sensor measurements gives 4 known values the inverse calculation should also be possible.

We define the 4 dimensional vector consisting of the measured sub-sensor forces as  $\mathbf{U}$ , the applied 3D force vector as  $\mathbf{f}$  and the theoretical sub-sensor forces shown in equation 8, which depends on the applied force as  $\mathbf{V}(\mathbf{f})$ . The goal is to find the vector  $\mathbf{f}$  which minimizes the error between  $\mathbf{U}$  and  $\mathbf{V}$  as defined in equation 9.

$$E = \|\mathbf{U} - \mathbf{V}(\mathbf{f})\| \quad (9)$$

Differentiating  $E$  with respect to  $x$ , cancels out all terms of  $y$  and  $z$  as shown in equation 10. The same happens when differentiating with respect to  $y$  and  $z$ . Solving these 3 equations for zero gives the force vector that minimizes the error. This is shown in equation 11.

$$\delta \frac{E}{\delta x} = 2\alpha(-e + w + 2\alpha x) \quad (10)$$

$$\mathbf{f} = \begin{pmatrix} x \\ y \\ z \end{pmatrix} = \begin{pmatrix} \frac{e-w}{2\alpha} \\ \frac{s-n}{2\alpha} \\ e + n + s + w \end{pmatrix} \quad (11)$$

### 3.5 Sub-conclusion

It was observed that the readings from the sensor keep growing if a constant force is applied. The same behavior was seen when a decreasing force was applied after the sensor had been subject to a very high force. This large settling time seems to be a characteristic of these types of sensors. If a force is applied in a short period, for example for detecting a surface normal, this large settling time might have little effect. But if the force is kept for a long period, for example when grasping and holding an object, it might be required to compensate for this effect.

The sensor output was linearized for forces below  $8N$  using the measurements obtained before the high force was applied, and thus with minimum error from the settling effect. The result was a first order function. A very simple model of the sensor able to calculate the expected sensor readings with a known force was derived. The same model was used to derive the opposite calculation, where the applied force could be calculated from the sensor readings. This model is very simple and based on many assumptions. It is unclear how precise it will be in practice and it has not been verified yet. But it could act as a base for further development of a more complex sensor model, which also take into consideration the location of the contact point.

## 4 Object Property Detection Experiments

One of the planned applications of the sensors is to explore the shape of an object, or in the simple case to detect the normal direction of a surface. A set of experiments was carried out to investigate whether these

two sensors were able to measure the normal of a surface by a single touch, and how precise the direction can be measured. Additionally two experiments were carried out to explore the ability of the *MicroJoystick* sensor to detect the weight and elasticity of an object being grasped.

#### 4.1 Definition of Surface direction

The direction of the surface in the experiments is defined relative to the orientation of the sensor itself. The direction of a surface is normally defined as a 3D vector, normal to the surface. This is not very useful in this case because the sensor might not be equally good at detecting how much the surface is tilted and in what direction it is tilted.

For this reason we define the orientation of the surface with two angles, the tilt angle  $\alpha$  and the roll angle  $\beta$ . Figure 14(b) shows the definition of the tilt angle. A tilt angle of  $\alpha = 0$  means the sensor is normal to the surface, and a positive tilt angle means the sensor is tilted towards the N direction.

Figure 14(c) shows the direction of the roll angle. A roll angle of  $\beta = 0$  gives a positive tilt in the N direction,  $\beta = \frac{\pi}{2}$  gives a tilt in the W direction and so on.

Using the ranges of the  $\alpha$  and  $\beta$  angles in equation 12 and 13 covers all possible orientations of a surface relative to the sensor when the sensor is pointing in the direction of the surface.

$$-\frac{\pi}{2} \leq \alpha \leq \frac{\pi}{2} \quad (12)$$

$$0 \leq \beta < \pi \quad (13)$$

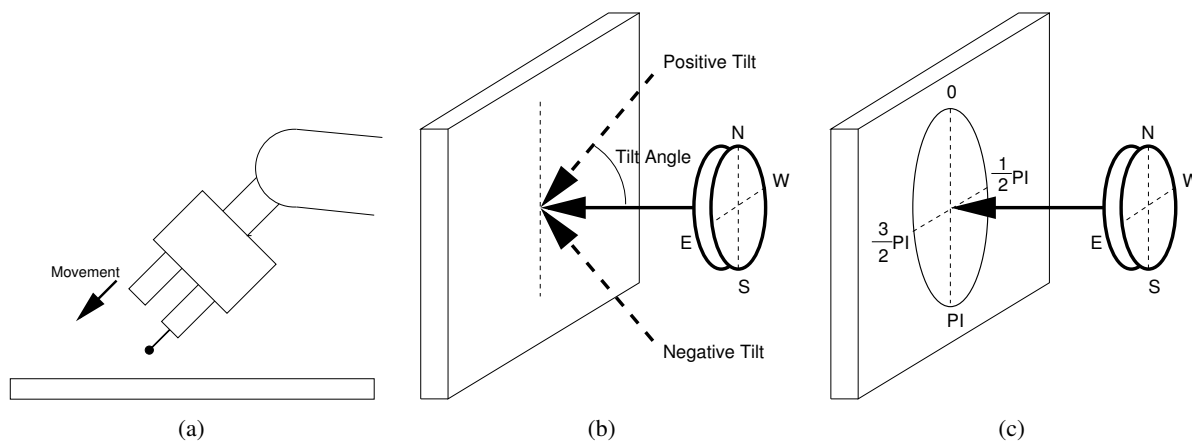


Figure 14: (a) Direction of the robot movement in the experiments. (b) The tilt angle used to define a surface orientation. (c) The roll angle used to define a surface orientation.

#### 4.2 Definition of Sensor Measurements

The measurement from each sensor is a 4 dimensional force vector  $\vec{S}$  consisting of the force measurement from each sub-sensor, shown in equation 14.

$$\vec{S} = \begin{pmatrix} n \\ s \\ e \\ w \end{pmatrix} \quad (14)$$

$$\hat{S} = \frac{\vec{S}}{|\vec{S}|} \quad (15)$$

$$\vec{D} = \begin{pmatrix} n - s \\ e - w \end{pmatrix} \quad (16)$$

$$\vec{P} = \begin{pmatrix} n - s \\ e - w \end{pmatrix} \cdot \frac{1}{|\vec{S}|} \quad (17)$$

Since the purpose of the sensor is to measure the orientation of a surface, we are interested in the difference between the opposite forces in each axis. We call the 2 dimensional vector representing this difference  $\vec{D}$ . It is defined in equation 16.

Since the contact between the sensor and the surface was done by placing the sensor in a steady position, the force applied by the robot arm to the sensor is unknown. The force can vary depending on how fast the robot was able to stop the movement after a contact was detected, the magnitude of the threshold force used to detect a contact and the velocity of the movement towards the surface.

To overcome this problem we assume that the relationship between the individual sub-sensor force measurements is constant for a given surface orientation, even if the total applied force is varied. By scaling the vector  $\vec{S}$  into a unit vector, it is thus possible to compare the sensor reading independent of the magnitude of the applied force. The vector consisting of the difference in each axis of the unit vector  $\vec{P}$  is defined as shown in equation 17. The vector  $\vec{P}$  will be used to detect the surface normal.

### 4.3 Surface Normal Detection Experiments

#### 4.3.1 Experimental setup

For this experiments one sensor was mounted on a robot finger. The surface used in the experiment was a wooden plate with plastic lamination. This gave a smooth surface, and some friction with the rubber tip of the sensor.

The orientation and position of the surface was known, and the sensor was moved in position above the surface, and repeatedly moved in contact with the surface from different directions. The movement towards the surface was made in a slow movement, following a straight line in 3D space in the direction parallel to the sensor, and keeping constant orientation as seen in figure 14(a). The movement had a velocity of approximately 1–2 mm per second. As soon as a force above a given threshold was detected from the sensor, the movement was stopped, and the position held for one second. Then the sensor was moved away from the surface again.

The following experiments were carried out:

1. Difference in applied force using the *MicroJoystick* sensor
2. Variations of tilt angle using the *MicroJoystick* sensor
3. Variations of roll and tilt angle using the *MicroJoystick* sensor
4. Variations of roll and tile angle using the *MicroNav* sensor

### 4.3.2 Experiment 1: Difference in applied force using the *MicroJoystick* sensor

In section 4.2 it was assumed that by scaling the measurement vector  $\vec{S}$  to unit length, the result was independent of the total force applied. The first experiment was made to verify the correctness of this, and to investigate how the measurements changed when the total applied force was varied.

This was done by creating contact with a surface from the same direction four times. The first time the movement was stopped when a force of 0.2 N was measured, the next time when 0.4 N was measured, 0.6 N and 0.8 N. This gave four different readings with the same surface orientation but different magnitude of applied force. The experiment was repeated seven times with different tilt angles in the range from  $0 \leq \alpha < \frac{\pi}{4}$  and a roll angle of  $\beta = 0$ .

The values of  $\vec{S}$  from each measurement are plotted as colored dots in figure 15(a). The measurements connected with a line were made with the same tilt angle. It is clear to see that the force values in general are higher in the four measurement in each group, than in the first.

The values of the unit vector  $\hat{S}$  are plotted the same way in figure 15(b) where the y-axis now corresponds to the force relative to the total force. The expected result would be that all values in the same group would have the same value, since they were done with the same tilt angle.

The values are not exactly the same, but it is still an improvement compared to figure 15(a). The standard deviation of all 28 groups of measurements were calculated to 0.018.

This is the expected standard deviation within the measurements when the magnitude of the total force is varied. Since the total sum of all four sensor values in the  $\hat{S}$  vector is 1.00, a standard deviation of 0.018 equals 1.8% which is a small error compared to other factors.

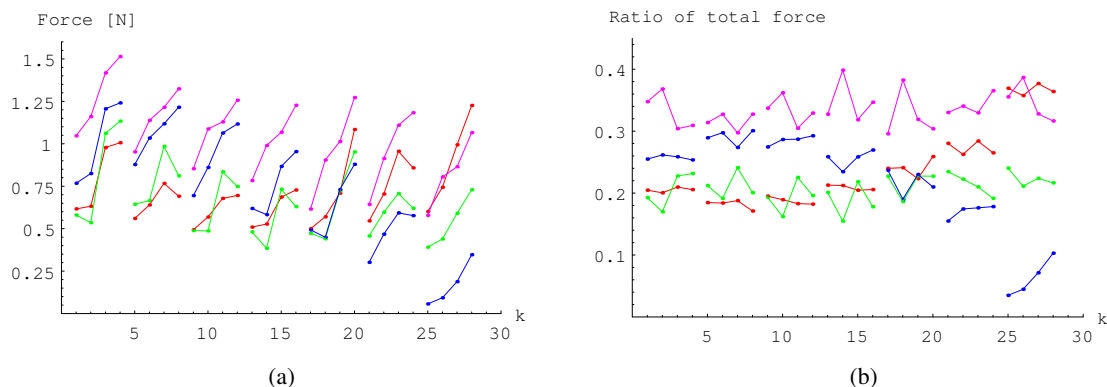


Figure 15: Results from experiment 1.  $k$  is the number of the measurement. Measurements done with the same tilt angle are connected with lines. Red=North, Blue=South, Green=East & Purple=West. (a) Measurements shown as force values. (b) Measurements shown as the ratio of the total force.

### 4.3.3 Experiment 2: Variations of tilt angle using the *MicroJoystick* sensor

The next experiment was made to investigate whether the sensor is able to detect variations in the tilt angle. The roll angle was kept constant at  $\beta = 0$ , and the sensor was moved into contact with a surface with the five tilt angles shown in eq. 18. For each tilt angle the experiment was repeated 10 times. This resulted in 50 measurements.

$$\alpha \in \left\{ 0, -\frac{1}{16}\pi, -\frac{2}{16}\pi, -\frac{3}{16}\pi, -\frac{4}{16}\pi \right\} \quad (18)$$

Since  $\beta$  is zero and  $\alpha$  negative, the sensor was tilted in the direction of the S sub-sensor. See figure 14(b).

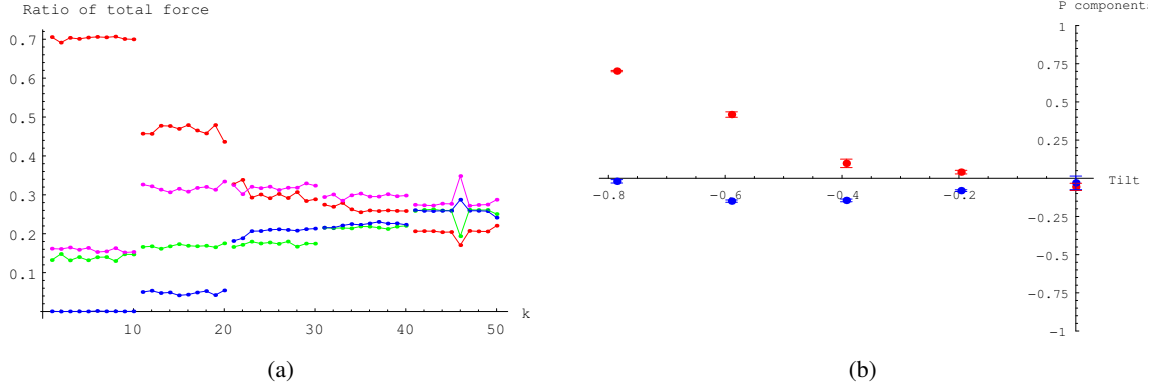


Figure 16: Results from experiment 2. **(a)** Measurements shown as the ratio of the total force.  $k$  is the number of the measurement. Measurements done with the same tilt angle are connected with lines. Red=North, Blue=South, Green=East & Purple=West. **(b)** Mean values of  $\vec{P}$  shown for the tested tilt angles. Red=North/South axis, Blue=East/West axis.

The result is plotted in figure 16(a). The mean of the 10 contacts done with each angle is listed in table 1. The standard deviation from the mean in the 10 contacts are listed in table 2. The average value of the standard deviations is 0.00886.

This standard deviation seems to be very small, which can also be seen by the almost horizontal lines in figure 16(a).

Tilt	N	E	S	W
$-\frac{4}{16}\pi$	0.702	0.139	0	0.158
$-\frac{3}{16}\pi$	0.466	0.168	0.048	0.318
$-\frac{2}{16}\pi$	0.302	0.174	0.205	0.319
$-\frac{1}{16}\pi$	0.264	0.216	0.223	0.297
0	0.204	0.253	0.26	0.283

Table 1: Results from the experiment with variations of the tilt angle. Each value is the mean value of the 10 measurements done.

Tilt	N	E	S	W
$-\frac{4}{16}\pi$	0.0046	0.007	0.0004	0.0049
$-\frac{3}{16}\pi$	0.0139	0.0039	0.0046	0.0084
$-\frac{2}{16}\pi$	0.0176	0.0048	0.0108	0.0076
$-\frac{1}{16}\pi$	0.008	0.0026	0.0048	0.0052
0	0.0126	0.0212	0.0111	0.0233

Table 2: The standard deviation in the measurements from the experiment with variations of the tilt angle.

To try to detect the tilt angle, we looked at the difference in each axis defined as the vector  $\vec{P}$  in section 4.2. This difference is listed in table 3(a), which was calculated by using the mean of the measurements from table 1. The standard deviation of the measurements from the mean is listed in table 3(b). The unit is of the same type as table 1 so the values can be directly compared. These values are plotted in figure 16(b). The sensor was tilted in the S-direction, which can be seen by a growing magnitude of the  $N - S$  value. The  $E - W$  would be expected to be constant zero.

Table 3: Result from experiment with variations in tilt angle. **(a)** Mean values of  $\vec{P}$  **(b)** Standard deviation in the measurements of  $\vec{P}$

(a)			(b)		
Tilt	N-S	E-W	Tilt	N-S	E-W
$-\frac{4}{16}\pi$	0.702	-0.02	$\frac{4}{16}\pi$	0.004	0.011
$-\frac{3}{16}\pi$	0.417	-0.15	$\frac{3}{16}\pi$	0.018	0.008
$-\frac{2}{16}\pi$	0.098	-0.145	$\frac{2}{16}\pi$	0.028	0.009
$-\frac{1}{16}\pi$	0.04	-0.081	$\frac{1}{16}\pi$	0.012	0.006
0	-0.056	-0.03	0	0.024	0.044

#### 4.3.4 Experiment 3: Variations of both roll and tilt angle using the *MicroJoystick* sensor

The experiment in section 4.3.3 was done with a constant roll angle of  $\beta = 0$ . This experiment will try to explore the behavior of the sensor when the roll angle is varied.

This was done by applying the tilt angles listed in eq. 19, with three different roll angles listed in eq. 20. Five measurements were taken for each angle, to be able to calculate the mean and the variance.

$$\alpha \in \left\{ 0, -\frac{1}{32}\pi, -\frac{2}{32}\pi, -\frac{3}{32}\pi, -\frac{4}{32}\pi, -\frac{5}{32}\pi, -\frac{6}{32}\pi, -\frac{7}{32}\pi, -\frac{8}{32}\pi \right\} \quad (19)$$

$$\beta \in \left\{ 0, \frac{1}{6}\pi, \frac{2}{6}\pi \right\} \quad (20)$$

The tilt angles are divided into smaller intervals than in the last experiment. It was not possible to apply tilt smaller than  $-\frac{5}{32}\pi$  when a roll angle of  $\frac{1}{6}\pi$  or  $\frac{2}{6}\pi$  was used. The reason for this is that the corner of the robot finger would hit the surface, so a higher tilt angle would require a different geometric design of the sensor setup.

The two components of the  $\vec{P}$  vector with a roll angle of  $\beta = 0$  are listed in table 4(a). Each of these values is the mean of five measurements done with the same angle. The standard deviations of these measurements are listed in table 4(b). These values are plotted in figure 17(a).

Table 4: Part of the result from experiment 3 with a roll angle of  $\beta = 0$  **(a)** Mean values of  $\vec{P}$  **(b)** Standard deviation in the measurements of  $\vec{P}$

(a)			(b)		
Tilt	N-S	E-W	Tilt	N-S	E-W
$\frac{8}{32}\pi$	0.68	-0.038	$\frac{8}{32}\pi$	0.006	0.013
$\frac{7}{32}\pi$	0.547	-0.042	$\frac{7}{32}\pi$	0.011	0.013
$\frac{6}{32}\pi$	0.343	-0.149	$\frac{6}{32}\pi$	0.009	0.008
$\frac{5}{32}\pi$	0.113	-0.15	$\frac{5}{32}\pi$	0.017	0.002
$\frac{4}{32}\pi$	0.07	-0.153	$\frac{4}{32}\pi$	0.026	0.009
$\frac{3}{32}\pi$	0.04	-0.093	$\frac{3}{32}\pi$	0.014	0.006
$\frac{2}{32}\pi$	0.029	-0.077	$\frac{2}{32}\pi$	0.029	0.009
$\frac{1}{32}\pi$	0.051	-0.04	$\frac{1}{32}\pi$	0.015	0.041
0	0.008	-0.049	0	0.013	0.02

Looking at the plot, the result looks similar to the results found in the previous experiment. The only difference between the two experiments was smaller step size in the tilt angle. With these smaller steps it is

more clearly to see that the value of  $N - S$  start growing significantly when the sensor is tilted more than  $0.4 \text{ rad}$  (about  $22^\circ$ ). For smaller tilt angles the behavior seems to be more random.

The same measurements, but with a roll angle of  $\beta = \frac{1}{6}\pi$  are listed in table 5(a), and the standard deviations are listed in table 5(b). The values are plotted in figure 17(b). The expected result would be that the  $E - W$  value is growing in the negative direction as the tilt angle becomes higher (seen from right to left in the plot) since the sensor is tilted slightly in the E-direction. Since the sensor is also tilted in the S-direction the value of  $N - S$  should also be growing although less than in the last experiment. Looking at figure 17(b) it is clear to see that this behavior is not quite as expected. The values are close to zero, changing sign randomly and the variance of the measurements is large compared to the values themselves. It is important to notice that the x-axis only goes down to  $-0.5$  where as in figure 17(a) it goes down to  $-0.8$ , because the hand was unable to tilt further in this setup.

Table 5: Part of the result from experiment 3 with a roll angle of  $\beta = \frac{1}{6}\pi$  (a) Mean values of  $\vec{P}$  (b) Standard deviation in the measurements of  $\vec{P}$

(a)			(b)		
Tilt	N-S	E-W	Tilt	N-S	E-W
$-\frac{0}{32}\pi$	0	-0.067	$-\frac{0}{32}\pi$	0.003	0.014
$-\frac{1}{32}\pi$	-0.029	-0.073	$-\frac{1}{32}\pi$	0.008	0.019
$-\frac{2}{32}\pi$	0.005	-0.003	$-\frac{2}{32}\pi$	0.013	0.007
$-\frac{3}{32}\pi$	0.014	0.048	$-\frac{3}{32}\pi$	0.007	0.038
$-\frac{4}{32}\pi$	0.07	0.024	$-\frac{4}{32}\pi$	0.013	0.056
$-\frac{5}{32}\pi$	0.08	-0.153	$-\frac{5}{32}\pi$	0.02	0.05

The means from the experiment with a roll angle of  $\beta = \frac{2}{6}\pi$  are listed in table 6(a), and the standard deviations listed in table 6(b). The result is plotted in figure 17(c). The expected result is a slightly growing value of  $N - S$  and a growing value of  $E - W$  in the negative direction, as the sensor is tilted. The result does not show this behavior. Instead the values seem to be close to zero with a high variance.

Table 6: Part of the result from experiment 3 with a roll angle of  $\beta = \frac{2}{6}\pi$  (a) Mean values of  $\vec{P}$  (b) Standard deviation in the measurements of  $\vec{P}$

(a)			(b)		
Tilt	N-S	E-W	Tilt	N-S	E-W
$-\frac{0}{32}\pi$	-0.007	-0.05	$-\frac{0}{32}\pi$	0.009	0.013
$-\frac{1}{32}\pi$	-0.02	-0.038	$-\frac{1}{32}\pi$	0.002	0.023
$-\frac{2}{32}\pi$	-0.037	0.028	$-\frac{2}{32}\pi$	0.009	0.037
$-\frac{3}{32}\pi$	-0.025	-0.014	$-\frac{3}{32}\pi$	0.018	0.074
$-\frac{4}{32}\pi$	-0.032	-0.049	$-\frac{4}{32}\pi$	0.029	0.074
$-\frac{5}{32}\pi$	0.031	0.002	$-\frac{5}{32}\pi$	0.052	0.058

#### 4.3.5 Experiment 4: Variations of both roll and tilt angle using the *MicroNav* sensor

The surface normal experiment were carried out again using the *MicroNav* sensor. For these experiments we used the same rubber tip that were originally mounted on the *MicroJoystick* sensor. This was glued to the *MicroNav* sensor as seen in figure 18. This makes it possible to get into contact with a surface even if it is not completely normal to the finger. To explore whether this new sensor design is able to measure the

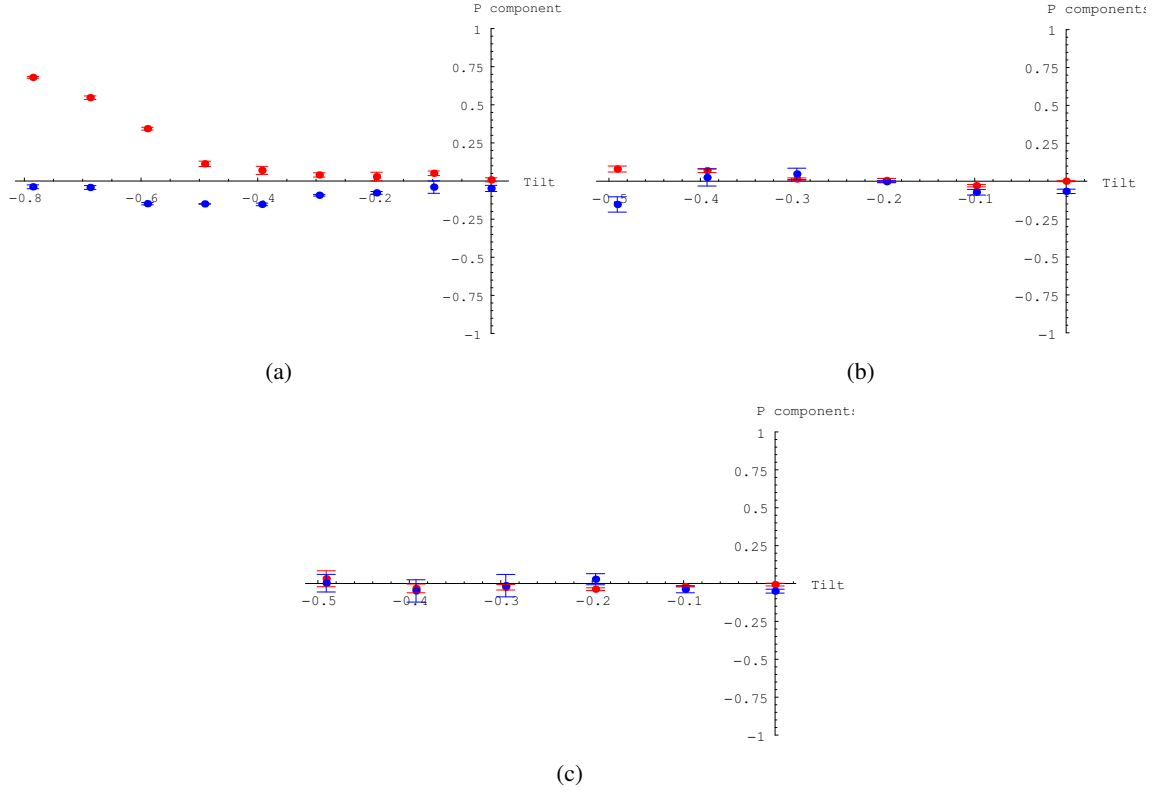


Figure 17: Results from experiment 3. Mean values of  $\vec{P}$  shown for the tested tilt angles. Red=North/South axis, Blue=East/West axis. **(a)** For a roll angle  $\beta = 0$ . **(b)** For a roll angle  $\beta = \frac{1}{6}\pi$ . **(c)** For a roll angle  $\beta = \frac{2}{6}\pi$ .

normal direction of a surface, we tested it with a series of contact angles. All possible pairs of the following roll and tilt angles were tested:

$$\alpha \in \left\{ 0, \frac{1}{32}\pi, \frac{2}{32}\pi, \frac{3}{32}\pi, \frac{4}{32}\pi, \frac{5}{32}\pi, \frac{6}{32}\pi \right\} \quad (21)$$

$$\beta \in \left\{ 0, \frac{1}{6}\pi, \frac{2}{6}\pi, \frac{3}{6}\pi \right\} \quad (22)$$

Each angle pair was tested six times to make it possible to measure both the mean value and the standard deviation. The difference in the two axes for a roll angle of  $\beta = 0$  is shown in table 7(a) and the standard deviation of the measurements are shown in table 7(b). A roll angle of  $\beta = 0$  means the sensor is tilted in the direction of the north sub-sensor. The results are also shown in figure 19(a), where the values have been subtracted with the values from a tilt angle of  $\alpha = 0$ . In practise this is done by calibrating the sensor by touching a surface directly normal to the sensor, and using these readings as zero.

The rest of the measurements with different roll angles, and the standard deviation of the measurements are listed in table 8(a)-10(b). These values are shown graphically in figure 19(b), 19(c) and 19(d). A roll angle of  $\beta = \frac{1}{2}\pi$  means the sensor is tilted in the direction of the west sub-sensor.

These results shows that the measured values from the sensor depends on both the roll and the tilt angle. A higher tilt angle gives a higher difference in the force readings for that respective axis which depends on the roll angle. It seems to be growing linear up to a point about  $0.4 \text{ rad}$  ( $22^\circ$ ) where the values seems to be

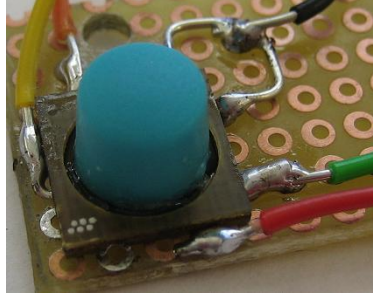


Figure 18: The MicroNav sensor with a mounted sensor tip.

become lower even when the tilt angle is higher. This shows that it should be possible to measure the roll and tilt angle for tilt angles lower than about  $22^\circ$  using the *MicroNav* sensor.

Table 7: Results from surface experiment with the *MicroNav* sensor using a roll angle of  $\beta = 0$ . (a) Mean values of  $\vec{P}$  (b) Standard deviation in the measurements of  $\vec{P}$

(a)			(b)		
Tilt	N-S	E-W	Tilt	N-S	E-W
$\frac{0}{32}\pi$	0.106	-0.206	$\frac{0}{32}\pi$	0.009	0.0358
$\frac{1}{32}\pi$	0.2	-0.211	$\frac{1}{32}\pi$	0.042	0.0306
$\frac{2}{32}\pi$	0.35	-0.196	$\frac{2}{32}\pi$	0.0291	0.0303
$\frac{3}{32}\pi$	0.439	-0.229	$\frac{3}{32}\pi$	0.0436	0.0266
$\frac{4}{32}\pi$	0.495	-0.219	$\frac{4}{32}\pi$	0.03	0.0104
$\frac{5}{32}\pi$	0.478	-0.235	$\frac{5}{32}\pi$	0.0127	0.0063
$\frac{6}{32}\pi$	0.417	-0.254	$\frac{6}{32}\pi$	0.0125	0.0094

#### 4.3.6 Discussion of Results

Experiment 2 shows that there is a good repeatability in the information received from the sensor when applied to a surface. Each orientation of the surface was touched 10 times with the sensor, and the average standard deviation of the measurements was only about 0.9% of the total force applied to the sensor. Experiment 1 shows that the repeatability is acceptable, even when the magnitude of the total force was varied. The average standard deviation in this case was found to be about 1.8% of the total force applied. In this experiment the variance in the measurements was provoked to be greater by changing the force on purpose, so this should be a worst case scenario.

Experiment 2 and 3 shows it should be possible to detect the tilt angle using the *MicroJoystick* sensor when the sensor is tilted with more than about  $22^\circ$ . For lower angles the values from the sensor are small compared to the deviation, so the measurements are very noisy. This noise could possibly be due to the friction force, which acts on the sensor tip in the tangential direction of the normal. Since the sensor was unable to reach the high tilt angles in experiment 3, it is unfortunately not possible to conclude how good the sensor is at detecting the roll angle.

Experiment 4 shows the *MicroNav* sensor can be used to detect the roll and tilt angle of a surface if the tilt angle is lower than about  $22^\circ$ .

Table 8: Results from surface experiment with the *MicroNav* sensor using a roll angle of  $\beta = \frac{1}{6}\pi$ . **(a)** Mean values of  $\vec{P}$  **(b)** Standard deviation in the measurements of  $\vec{P}$

(a)			(b)		
Tilt	N-S	E-W	Tilt	N-S	E-W
$\frac{0}{32}\pi$	0.106	-0.206	$\frac{0}{32}\pi$	0.009	0.0358
$\frac{1}{32}\pi$	0.203	-0.216	$\frac{1}{32}\pi$	0.016	0.0407
$\frac{2}{32}\pi$	0.32	-0.335	$\frac{2}{32}\pi$	0.0465	0.0319
$\frac{3}{32}\pi$	0.418	-0.338	$\frac{3}{32}\pi$	0.0242	0.0263
$\frac{4}{32}\pi$	0.422	-0.388	$\frac{4}{32}\pi$	0.0404	0.0169
$\frac{5}{32}\pi$	0.44	-0.405	$\frac{5}{32}\pi$	0.0338	0.047
$\frac{6}{32}\pi$	0.354	-0.388	$\frac{6}{32}\pi$	0.0128	0.0279

Table 9: Results from surface experiment with the *MicroNav* sensor using a roll angle of  $\beta = \frac{2}{6}\pi$ . **(a)** Mean values of  $\vec{P}$  **(b)** Standard deviation in the measurements of  $\vec{P}$

(a)			(b)		
Tilt	N-S	E-W	Tilt	N-S	E-W
$\frac{0}{32}\pi$	0.106	-0.206	$\frac{0}{32}\pi$	0.009	0.0358
$\frac{1}{32}\pi$	0.15	-0.321	$\frac{1}{32}\pi$	0.0533	0.0055
$\frac{2}{32}\pi$	0.246	-0.436	$\frac{2}{32}\pi$	0.0218	0.0237
$\frac{3}{32}\pi$	0.282	-0.483	$\frac{3}{32}\pi$	0.0351	0.046
$\frac{4}{32}\pi$	0.294	-0.458	$\frac{4}{32}\pi$	0.0223	0.0417
$\frac{5}{32}\pi$	0.304	-0.492	$\frac{5}{32}\pi$	0.0687	0.0523
$\frac{6}{32}\pi$	0.307	-0.507	$\frac{6}{32}\pi$	0.0257	0.074

Table 10: Result from surface experiment with the *MicroNav* sensor with a roll angle of  $\beta = \frac{3}{6}\pi$ . **(a)** Mean values of  $\vec{P}$  **(b)** Standard deviation in the measurements of  $\vec{P}$

(a)			(b)		
Tilt	N-S	E-W	Tilt	N-S	E-W
$\frac{0}{32}\pi$	0.106	-0.206	$\frac{0}{32}\pi$	0.009	0.0358
$\frac{1}{32}\pi$	0.082	-0.29	$\frac{1}{32}\pi$	0.0159	0.0664
$\frac{2}{32}\pi$	0.211	-0.407	$\frac{2}{32}\pi$	0.0211	0.0203
$\frac{3}{32}\pi$	0.211	-0.518	$\frac{3}{32}\pi$	0.0364	0.058
$\frac{4}{32}\pi$	0.22	-0.577	$\frac{4}{32}\pi$	0.0324	0.0246
$\frac{5}{32}\pi$	0.238	-0.593	$\frac{5}{32}\pi$	0.0485	0.0558
$\frac{6}{32}\pi$	0.222	-0.582	$\frac{6}{32}\pi$	0.0295	0.0603

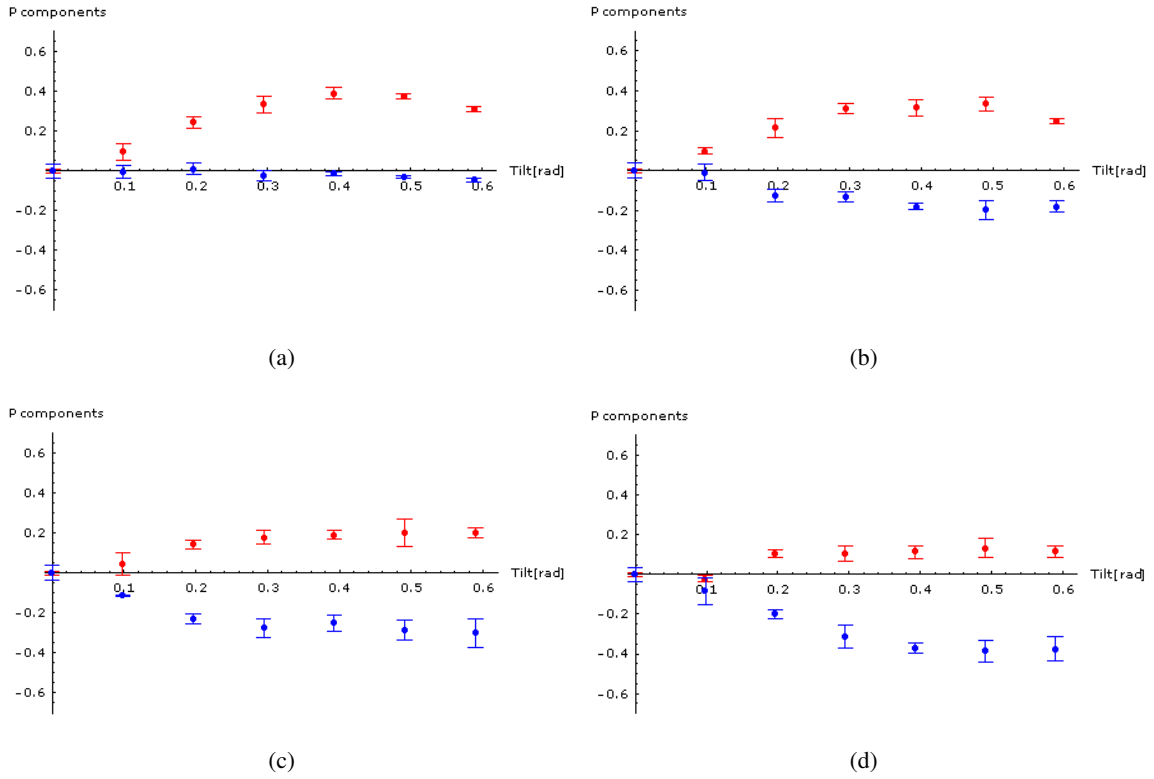


Figure 19: Results from surface normal experiment using the *MicroNav* sensor. Mean values of  $\vec{P}$  shown for the tested tilt angles. Red=North/South axis, Blue=East/West axis. **(a)** For a roll angle  $\beta = 0$ . **(b)** For a roll angle  $\beta = \frac{1}{6}\pi$ . **(c)** For a roll angle  $\beta = \frac{2}{6}\pi$ . **(d)** For a roll angle  $\beta = \frac{3}{6}\pi$ .

#### 4.4 Elasticity Experiment

The elasticity of an object or a surface is the ability to deform when a force is applied to a contact point, for example during a grasp. The elasticity is a useful property to be known in grasping, since it makes it possible to predict in what way the object will deform during a grasp. It is also a relevant object property. A high elasticity makes an object for example useless to be used in a hammer like way. The ability of the sensor to measure the elasticity of an object was explored using a two sensor setup mounted on a parallel gripper. The gripper would close around a plastic cup with the two sensors as the only contact points. When the cup was grasped in the top it would deform into an oval shape, since it is more flexible at this point (see figure 20(a)). In the lower part of the cup the shape was stabilized by the bottom of the cup, and would not easily deform (see figure 20(b)). The parallel gripper was closed slowly with a constant velocity and stopped when a certain maximum force was reached. The diameter of the cup at the top was a little larger than at the bottom. It is 59 mm at the top versus 57.5 mm at the bottom. The experiment was repeated five times with different contact locations. The force measured by one of the sensors as the gripper was closing can be seen in figure 20(c). The light blue graph shows the result when the contact point was at the top of the cup, and the red graph shows for the bottom of the cup. The rest of the graphs show the contact points in between these two.

It can clearly be seen that the force is growing slowly when grasping at a soft location, and growing fast when grasping at a hard location. The sensor is also able to detect the different diameter of the cup, de-

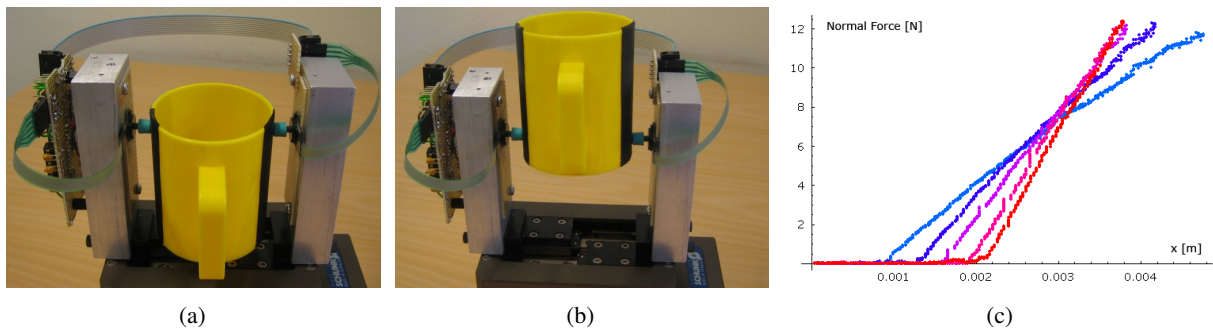


Figure 20: Elasticity Experiment Setup **(a)** The cup grasped at the top. **(b)** The cup grasped at the bottom. **(c)** Results from the experiment. Light Blue = grasp located at the top, Red = grasp located at the bottom, Other colors = grasp located in between

pending on the grasping point. When grasping at the top the sensor measures a contact after about 1 mm of movement, and when grasping at the bottom it measures a contact after about 2 mm of movement because of the smaller diameter.

#### 4.5 Weight Experiment

The sensors are not expected to be able to measure the precise weight of an object, but we find it useful to investigate whether they are able to give an indication of the weight of a grasped object to attach properties such as 'fullness' or 'emptiness'. For this experiment the same sensor setup was used, and the sensor readings were recorded while objects with constant shape but different weights were grasped. The gravitational force would exert a downwards force on the object, so the weight was expected to be measurable in the force readings in vertical axis of the sensor. The plastic cup was grasped one time where it was empty (see figure 21(a)) and several times filled with different amounts of metal objects (see figure 21(b)).

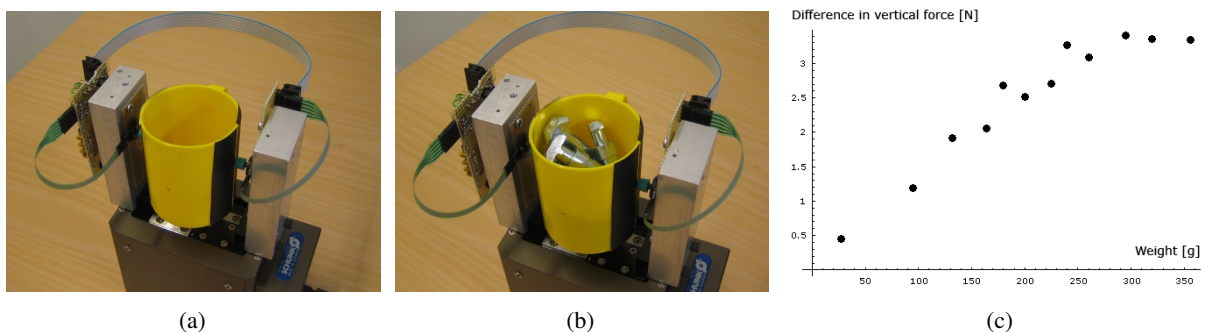


Figure 21: Weight Experiment Setup **(a)** Empty Cup. **(b)** Full Cup. **(c)** Results from the experiment.

The result can be seen in figure 21(c). The y-axis shows the average of the force difference measured in the vertical direction of the two sensors. This value seems to depend linearly on the weight of the object except for weights higher than about 300 g, where it seems to approach a limit.

## 5 Multisensorial surface exploration

This experiment shows that the sensor can be used to verify whether a surface predicted by the vision system actually exists. The visual prediction of surfaces is described in [5]. The scene chosen for verification consists of the closed white box placed on a black surface (see figure 22(a)). The vision system predicts three possible surfaces in the scene. A surface on the top of the box, a surface on the side of the box and a surface between the edge of the box and the edge of the black surface (see figure 22(b)).

Each of these three detected surfaces consist of a group of visual mono primitives each describing among other things the position of a point on the surface and the surface normal in that point. Using this information from a visual mono it is possible to create a movement where the sensor is moved through a point on the predicted surface in a linear movement parallel to the surface normal. The verification of a surface is done by choosing one of more mono primitives on the surface for verification.

Figure 22(c) shows a situation where a visual mono on the top of the box has been chosen. The robot moves the gripper in position above the surface, and then does a straight line movement through the surface. When a contact is detected by the sensor (see figure 22(d), the movement is stopped and a haptic mono primitive is added at the point of contact. This haptic contact can now be used to measure the normal direction of the surface and other surface properties in that single point.

The top surface of the box was verified three times, resulting in three haptic mono primitives which can be seen in figure 22(e). Each haptic primitive is shown as a red square marking the position, and a green line marking the surface normal.

The vision system also predicted a surface located between the edge of the box and the edge of the black surface. To verify this surface a visual mono was chosen and the robot did the same straight line movement though the predicted surface. Since no surface exist in the point the robot moves through the predicted surface without detecting a contact and stops when a maximum distance has been reached (see figure 22(f)). Since the visual mono primitives on the same surface are grouped together it is now possible to remove all the monos from this wrongly predicted surface.

## 6 Conclusion

We have shown that it is possible to extract object information such as surface normal, weight and elasticity using the *MicroJoystick* and *MicroNav* sensors from Interlink electronics. By this we have demonstrated the usability of these sensors for tasks such as haptic exploration and grasping.

## Acknowledgment

This work is supported by the PACO-PLUS project.

## References

- [1] Interlink electronics. <http://www.interlinkelec.com>.
- [2] Pressure Profile Systems Inc. <http://www.pressureprofile.com>.
- [3] Tekscan. <http://www.tekscan.com>.
- [4] Weiss robotics. <http://www.weiss-robotics.de/>.

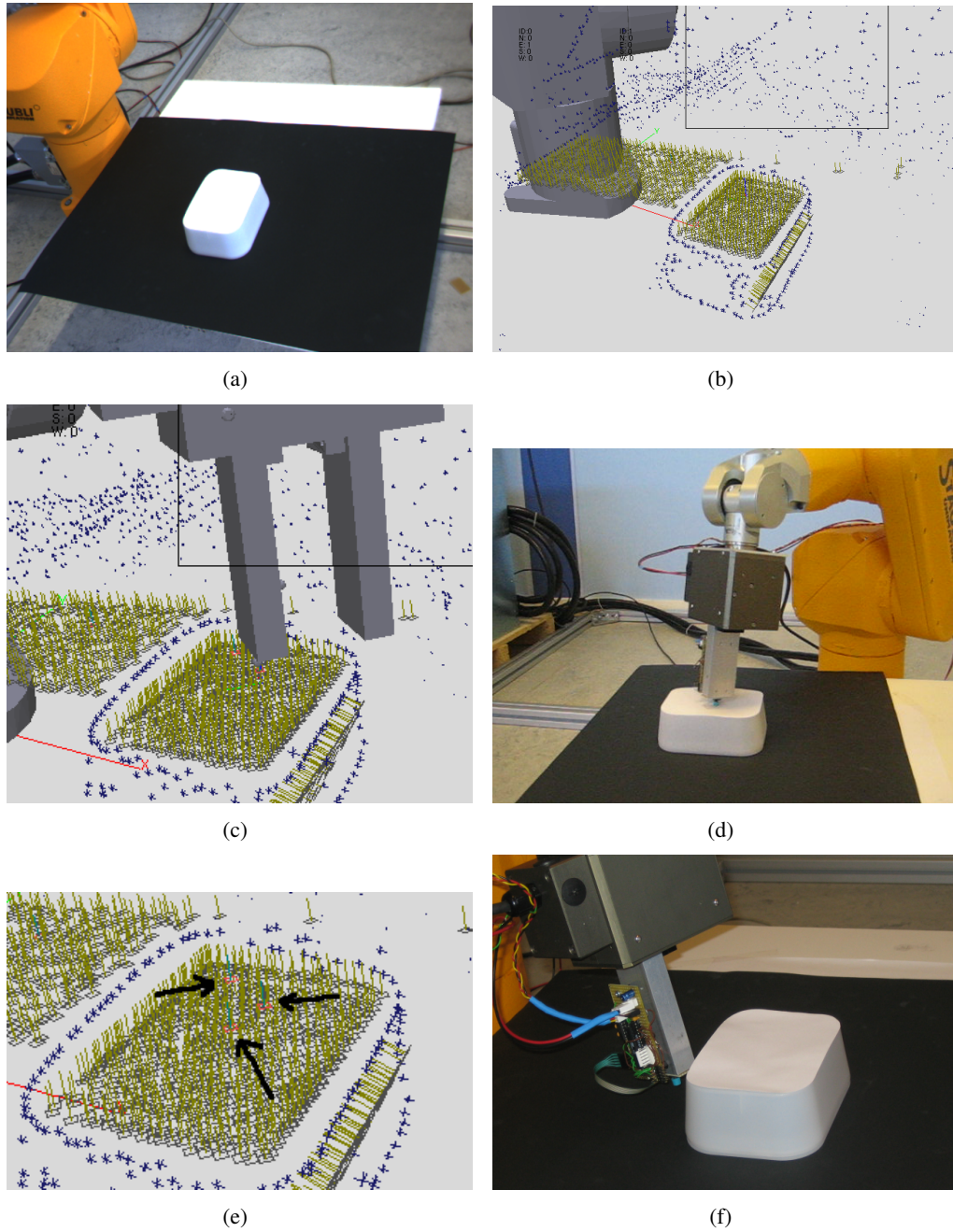


Figure 22: Surface Verification Experiment. **(a)** Setup of the scene. **(b)** View of the 3 predicted surfaces. **(c)** The robot moving in position to verify the surface on the box. **(d)** The sensor in contact with the surface on the box. **(e)** The 3 detected haptic primitives shown as small red squares. **(f)** The robot moving through the wrongly predicted surface without detecting a contact.

- [5] S. Kalkan, F. Wörgötter, and N. Krüger. Depth prediction at homogeneous image structures. In *Technical report of the Robotics Group, Maersk Institute, University of Southern Denmark*, number 2007-2, 2007.
- [6] S. Schulz, C. Pylatiuk, and G. Bretthauer. A new ultralight anthropomorphic hand. In *Internat. Conf. on Robotics and Automation 2001, Seoul, Korea*, 2001.
- [7] Stuart I. Yaniger. Force Sensing Resistors: A Review of the Technology. *Electro International*, pages 666–668, 1991.